Passivity-Based Stability Assessment of Grid-Connected VSCs - An Overview

Harnefors, Lennart; Wang, Xiongfei; Yepes, Alejandro G.; Blaabjerg, Frede

Published in:
I E E E Journal of Emerging and Selected Topics in Power Electronics

DOI (link to publication from Publisher):
10.1109/JESTPE.2015.2490549

Publication date:
2016

Document Version
Accepted author manuscript, peer reviewed version

Passivity-Based Stability Assessment of Grid-Connected VSCs—An Overview

Lennart Harnefors, *Senior Member, IEEE*, Xiongfei Wang, *Member, IEEE*, Alejandro G. Yepes, *Member, IEEE*, and Frede Blaabjerg, *Fellow, IEEE*

Abstract— **The interconnection stability of a grid-connected voltage-source converter (VSC) can be assessed by the passivity properties of the VSC input admittance. If critical grid resonances fall within regions where the input admittance acts passively, i.e., has nonnegative real part, then their destabilization is generally prevented. This paper presents an overview of passivity-based stability assessment, including techniques for space-vector modeling of VSCs whereby expressions for the input admittance can be derived. Design recommendations for minimizing the negative-real-part region are given as well.**

Index Terms— **Converter control, passivity, resonances, stabilization.**

I. Introduction

THE PENETRATION of grid-connected converters, particularly voltage-source converters (VSCs), is currently rising rapidly [1]. As a consequence, the risk increases for destabilization of critical grid resonances [2]–[23]. These are resonances that are poorly damped and electrically located close to one VSC, or multiple VSCs, of high enough power rating in relation to the short-circuit ratio (SCR) of the grid.

Stability of a system comprising multiple grid-connected VSCs is generally difficult to analyze (e.g., using eigenvalues [13] or the Nyquist criterion [16]), particularly if the VSCs have different ratings and dynamic properties. On the other hand, the frequency-domain passivity theory offers an effective method for stability assessment [2]–[7].

Suppose that all VSCs, as well as all other power-system components, have a passive behavior, i.e., the real part of the input admittance (also called the conductance) is nonnegative for all frequencies. Then, the system is guaranteed to be stable regardless of the number of converters, because a network that consists solely of passive components—no matter how complex—is always stable.

However, the pure passivity of all components is impossible to obtain. VSCs have negative-conductance behavior in certain frequency ranges [2]. So do electrical machines (due to the induction generator effect [24]). Yet, if it can be ascertained that every grid-connected VSC has a nonnegative conductance in frequency regions where critical grid resonances appear—i.e., partial passivity—then it is unlikely that the VSCs will induce resonance destabilization. Grid codes based on this concept are enforced by several European administrations of electrified railways. It is typically required that nonnegative conductance above the fifth-harmonic frequency must be demonstrated for any new or retrofitted active-front-end rail vehicle to be approved [25], [26].

The main objective of this paper is to make a comprehensive overview of the passivity properties of the VSC input admittance. Important previously found results are highlighted. Modeling methods of three-phase VSCs for grid-interaction studies are reviewed, and design recommendations for minimizing the negative-real-part regions are given.

The stage is set in Section II, where a review of critical grid resonances is made, and the details of the assumed VSC control system are discussed. The passivity properties of the so-called inner input admittance, which results from just the current controller (CC) and the pulsewidth modulator (PWM), are considered in Section III. Requirements on the controller parameters and on the total time delay for obtaining passivity are presented. In Section IV, the consideration is extended to the total input admittance, which includes the impact of outer loops that feed into the CC, i.e., the phase-locked loop (PLL) and the direct-voltage controller (DVC). Here, the main novel result of this paper appears. It is shown how complex space vectors and complex transfer functions can be applied to assess the passivity properties of the total input admittance (even though the latter is dq imbalanced [27]). The analysis method has similarities to that suggested in [10], [15], and [17], but the impact of the DVC is included in addition to the impact of the PLL. Moreover, the usage of space vectors rather than phase quantities obviates the need for deriving separate positive- and negative-sequence expressions.

II. Preliminaries

A. Critical Grid Resonances

Grid resonances that are vulnerable to destabilization by VSCs can broadly be classified into two categories.

Manuscript received May 20, 2015; revised August 31, 2015; accepted October 11, 2015. Date of publication October 14, 2015; date of current version January 29, 2016. This work was supported in part by ABB, in part by the European Research Council through the European Union's Seventh Framework Program FP7/2007-2013 under Grant 321149, in part by the Spanish Ministry of Science and Innovation, and in part by the European Commission through the European Regional Development Fund under Project DPI2012-31283. Recommended for publication by Associate Editor Q.-C. Zhong.

L. Harnefors is with ABB, Corporate Research, Västerås 72178, Sweden (e-mail: lennart.harnefors@se.abb.com).

X. Wang and F. Blaabjerg are with the Department of Energy Technology, Aalborg University, Aalborg 9220, Denmark (e-mail: xwa@et.aau.dk; fbl@et.aau.dk).

A. G. Yepes is with the Department of Electronics Technology, University of Vigo, Vigo 36310, Spain (e-mail: agyepes@uvigo.es).

Color versions of one or more of the figures in this paper are available online at http://ieeexplore.ieee.org.

Digital Object Identifier 10.1109/JESTPE.2015.2490549

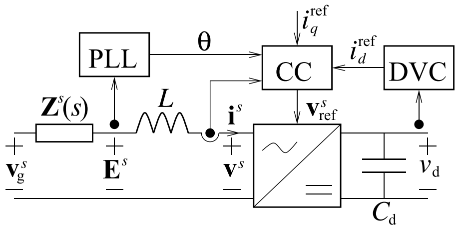

Fig. 1. VSC circuit and control-system block diagram.

1) Harmonic Resonances: Resonances in this category appear in the range from hundreds of hertz up to a few kilohertz. The first incident of harmonic resonance destabilization, as known to the authors, occurred in the Swiss single-phase rail grid in 1995 [28]–[31]. Harmonic resonances are caused by the inherent impedance characteristics of power lines and cables, often in conjunction with converter input filters, such as inductance–capacitance–inductance (*LCL*) filters.

2) Near-Synchronous Resonances: In this category, we find resonances in the range from the synchronous (fundamental) frequency f_1 up to roughly $2f_1$, which typically appear in very weak grids, i.e., with an SCR approaching 1 p.u. [32]. Subsynchronous resonances [33], i.e., below f_1, can be classified in this category as well.

B. Causes of Resonance Destabilization

The causes of negative-conductance behavior of a VSC (in turn, possibly leading to resonance destabilization) are as follows:

1) the total, i.e., computation-plus-PWM, time delay T_d;
2) the CC dynamics;
3) the dynamics of the outer controllers, i.e., the PLL and, provided that such are used, the DVC and the controller for the reactive power or the point-of-common-coupling (PCC)-voltage magnitude.

Causes 1) and 2) affect harmonic resonances, whereas causes 2) and 3) affect near-synchronous resonances.

C. System Model

In the following, the positive- and negative-sequence synchronous components are, for convenience, referred to as $+1$ and -1, respectively. Harmonics are referred to with their signed order in a similar fashion. Boldface letters are used to denote complex space vector and transfer functions that operate on complex space vectors. The derivative operator is denoted by $s = d/dt$ (which shall be considered as the complex Laplace variable, where appropriate). Vectors and transfer functions referred to the stationary $\alpha\beta$ frame are denoted with the superscript s, whereas vectors and transfer functions referred to the synchronous dq frame aligned with $+1$ are denoted without a superscript. We introduce $T_s = 1/f_s$ as the sampling period, and $\omega_1 = 2\pi f_1$ and $\omega_s = 2\pi f_s$ as the angular synchronous and angular sampling frequencies, respectively.

In the control system, the CC closes the innermost, and fastest, loop for the converter current $\mathbf{i}^s$ (see Fig. 1). Overmodulation is assumed not to occur, and switching harmonics are disregarded, allowing the PWM process to be modeled as lumped with the computational time delay into the total time delay T_d. The converter is assumed to be equipped with an inductive input filter, with inductance L and a negligible resistance. Hence, the converter-current dynamics are in the $\alpha\beta$ frame governed by

$$\mathbf{i}^s = \frac{\mathbf{E}^s - \mathbf{v}^s}{sL}, \quad \mathbf{v}^s = e^{-sT_d}\mathbf{v}_{\text{ref}}^s \tag{1}$$

where $\mathbf{E}^s$ is the PCC voltage and $\mathbf{v}_{\text{ref}}^s$ is the reference vector to the PWM, by which the converter voltage $\mathbf{v}^s$ is generated. The dq-frame correspondence is obtained simply by substituting $s \to s + j\omega_1$ [27]

$$\mathbf{i} = \frac{\mathbf{E} - \mathbf{v}}{(s + j\omega_1)L}, \quad \mathbf{v} = e^{-(s+j\omega_1)T_d}\mathbf{v}_{\text{ref}}. \tag{2}$$

The grid impedance $\mathbf{Z}^s(s)$, which is assumed to be balanced (also known as symmetric [27]), adds the following relations in the $\alpha\beta$ and dq frames, respectively:

$$\mathbf{v}_g^s - \mathbf{Z}^s(s)\mathbf{i}^s = \mathbf{E}^s \qquad \mathbf{v}_g - \mathbf{Z}(s)\mathbf{i} = \mathbf{E} \tag{3}$$

where $\mathbf{Z}(s) = \mathbf{Z}^s(s + j\omega_1)$ and $\mathbf{v}_g^s$ is the stiff grid voltage. The PLL and the DVC feed into the CC with signals θ and i_d^{ref}, respectively (see Section II-E for details). From these signals, together with i_q^{ref}, the $\alpha\beta$-frame converter-current reference is formed as $\mathbf{i}_{\text{ref}}^s = e^{j\theta}(i_d^{\text{ref}} + j i_q^{\text{ref}})$. The DVC has as input the dc-link voltage v_d, which is measured across the dc-link capacitor (with capacitance C_d).

D. CC

The two CC options that most frequently are suggested in the literature are here reviewed.

1) dq-Frame CC: The CC is in this case given by

$$\mathbf{v}_{\text{ref}} = -e^{j\omega_1 T_d}[\mathbf{F}_c(s)(\mathbf{i}_{\text{ref}} - \mathbf{i}) + j\omega_1 L\mathbf{i}] \tag{4}$$

where $\mathbf{F}_c(s)$ is the controller transfer function and the angle-adjustment factor $e^{j\omega_1 T_d}$ compensates the angle-displacement factor $e^{-j\omega_1 T_d}$ in (2). For brevity, PCC-voltage feedforward [3] is not included, but a dq decoupling term $j\omega_1 L\mathbf{i}$ is added. This prioritizes control of $+1$ over -1.

A proportional (P)-plus-resonant (R) controller with reduced-order generalized integrators (ROGIs) [34] as R parts is a suitable choice

$$\mathbf{F}_c(s) = \alpha_c L\left(1 + \sum_h \frac{\alpha_h e^{j\phi_h}}{s - jh\omega_1}\right) \tag{5}$$

where α_c is the ideal closed-loop-system bandwidth, α_h (with dimension angular frequency) is the individual gain factor of the R part for the harmonic order h, and ϕ_h is the compensation angle of that R part [35], [36]. Characteristically, R parts are included for $+1$ and -1 as well as for balanced harmonics, i.e., orders $-5, +7, -11, +13\ldots$ [34]. These translate to $h = 0, -2, \pm 6, \pm 12, \ldots$ in the dq frame. The R part at $h = 0$ reduces to a pure integrator. Selecting $\alpha_h \ll \alpha_c$ is recommended [37].

Combining (2) and (4) yields

$$\mathbf{i} = \mathbf{G}_{\mathrm{ci}}(s)\mathbf{i}_{\mathrm{ref}} + \mathbf{Y}_i(s)\mathbf{E} \tag{6}$$

where the inner closed-loop system and the inner input admittance, respectively, are given by

$$\mathbf{G}_{\mathrm{ci}}(s) = \frac{e^{-sT_d}\mathbf{F}_c(s)}{[s + j\omega_1(1 - e^{-sT_d})]L + e^{-sT_d}\mathbf{F}_c(s)} \tag{7}$$

$$\mathbf{Y}_i(s) = \frac{1}{[s + j\omega_1(1 - e^{-sT_d})]L + e^{-sT_d}\mathbf{F}_c(s)}. \tag{8}$$

By inner, it is meant that the outer control loops, i.e., the PLL and the DVC, are not yet considered. Owing to the dq decoupling and the angle-adjustment factor, $\mathbf{G}_{\mathrm{ci}}(0) = 1$ irrespective of $\mathbf{F}_c(0)$.

Remark 1: In (5), each ROGI pair at $h = \pm 6, \pm 12, \ldots$ can, provided that $\alpha_{-h} = \alpha_h$ and $\phi_{-h} = -\phi_h$, be merged into a second-order generalized integrator (SOGI) [35], [36] as

$$\frac{\alpha_h e^{j\phi_h}}{s - jh\omega_1} + \frac{\alpha_h e^{-j\phi_h}}{s + jh\omega_1} = 2\alpha_h \frac{s\cos\phi_h - h\omega_1 \sin\phi_h}{s^2 + (h\omega_1)^2}. \tag{9}$$

This reduces the total computational burden, since complex coefficients are avoided. If desired, the ROGI for -1 (i.e., $h = -2$) can be replaced by an SOGI with $h = 2$ according to the right-hand side of (9).

2) $\alpha\beta$-Frame CC: An equivalent $\alpha\beta$-frame implementation of control law (4) can be obtained simply by substituting $s \to \tilde{s}$, where

$$\tilde{s} = s - j\omega_1. \tag{10}$$

We get

$$\mathbf{v}^s_{\mathrm{ref}} = -e^{j\omega_1 T_d}\big[\mathbf{F}_c(\tilde{s})\big(\mathbf{i}^s_{\mathrm{ref}} - \mathbf{i}^s\big) + j\omega_1 L\mathbf{i}^s\big]. \tag{11}$$

The correspondences to (7) and (8) too are obtained simply by substituting $s \to \tilde{s}$

$$\mathbf{G}^s_{\mathrm{ci}}(s) = \frac{e^{-\tilde{s}T_d}\mathbf{F}_c(\tilde{s})}{(s - j\omega_1 e^{-\tilde{s}T_d})L + e^{-\tilde{s}T_d}\mathbf{F}_c(\tilde{s})} \tag{12}$$

$$\mathbf{Y}^s_i(s) = \frac{1}{(s - j\omega_1 e^{-\tilde{s}T_d})L + e^{-\tilde{s}T_d}\mathbf{F}_c(\tilde{s})}. \tag{13}$$

Remark 2: It should be observed that the angle-adjustment factor and the dq decoupling term remain in (11), which is not common practice in $\alpha\beta$-frame control. However, both are useful in this case as well, as they for $+1$ compensate the static voltage drop $j\omega_1 L\mathbf{i}^s$ across the filter inductor, thus giving prioritized control of $+1$. As a result, $\mathbf{G}^s_{\mathrm{ci}}(j\omega_1) = 1$ irrespective of $\mathbf{F}_c(0)$.

Remark 3: Notice that, even for $\alpha\beta$-frame implementation, controller (5) is designed as referred to the dq frame, i.e., with $h = 0, -2, \pm 6, \ldots$. It is then transformed to the $\alpha\beta$ frame by the substitution $s \to \tilde{s} = s - j\omega_1$.

Remark 4: For $\alpha\beta$-frame control, the ROGIs for ± 1 can be merged into an SOGI according to (9). However, replacing the ROGIs for harmonics with SOGIs only adds to the computational burden, as the system order doubles for each controlled harmonic [34].

3) Bandwidth Selection: The following two assumptions allow a simplified stability analysis of the current control loop to be carried out: 1) The R parts have negligible impact (which is reasonable, given the aforementioned recommendation $\alpha_h \ll \alpha_c$). 2) The imperfect dq decoupling that results from the time delay can be neglected, i.e., $1 - e^{-sT_d} \approx 0$. Then, $\mathbf{G}_{ci}(s) = \mathbf{G}_k(s)/[1 + \mathbf{G}_k(s)]$, where

$$\mathbf{G}_k(s) = \frac{\alpha_c e^{-sT_d}}{s} \tag{14}$$

is the open-loop transfer function. Since $|\mathbf{G}_k(j\alpha_c)| = 1$, α_c is the crossover frequency. Thus, the phase margin is given by

$$\phi_m = \pi + \arg \mathbf{G}_k(j\alpha_c) = \frac{\pi}{2} - \alpha_c T_d. \tag{15}$$

With the total time delay expressed in the sampling period as $T_d = nT_s = 2\pi n/\omega_s$, a bandwidth selection recommendation can be obtained as

$$\alpha_c \leq \left(\frac{\pi}{2} - \phi_m\right)\frac{\omega_s}{2\pi n}. \tag{16}$$

The selection recommendation $\alpha_c \leq \omega_s/10$ of [38] is obtained as a special case of (16), e.g., for $\phi_m = \pi/5 = 36°$ and $n = 1.5$.

E. Outer Control Loops

To save space, the loop that, via i_q^{ref}, controls the reactive power or the PCC-voltage magnitude is disregarded, and a constant i_q^{ref} is considered (see Fig. 1).

1) PLL: The purpose of the PLL is to track the rotation of the PCC voltage vector, thereby aligning the dq frame (with angle θ relative the $\alpha\beta$ frame) with the $+1$ component of $\mathbf{E}^s$, whose magnitude is E_0. The PLL uses the imaginary part of $\mathbf{E} = e^{-j\theta}\mathbf{E}^s$ as input signal, which is fed to the PLL controller $F_p(s)$. This is typically a P–integral controller, which can be expressed as

$$F_p(s) = \frac{\alpha_p}{E_0}\left(1 + \frac{\alpha_{\mathrm{ip}}}{s}\right) \tag{17}$$

where the normalization of the input signal is made by the division by E_0, and where the gains (with dimension angular frequency) typically are selected as $\alpha_{\mathrm{ip}} < \alpha_p \ll \alpha_c$. To the PLL-controller output, ω_1 is added, and the sum signal is then integrated to form the transformation angle as

$$\theta = \frac{1}{s}[F_p(s)\mathrm{Im}\{\mathbf{E}\} + \omega_1]. \tag{18}$$

The PLL thus forces $\mathrm{Im}\{\mathbf{E}\}$ to zero in the steady state (disturbances disregarded), leaving $\mathbf{E} = E_0$. Assuming power-invariant space-vector scaling or per unit values, the complex converter input power is given by $\mathbf{S} = \mathbf{E}\mathbf{i}^*$ [39]. With $\mathbf{E} = E_0$, we thus have

$$\mathbf{S} = P + jQ = E_0(i_d - ji_q) \tag{19}$$

which shows that i_d and $-i_q$ are the active-power-producing and reactive-power-producing current components, respectively.

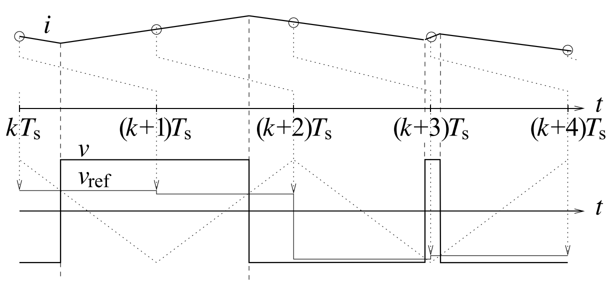

Fig. 2. Double-update PWM, giving $T_d = 1.5T_s$.

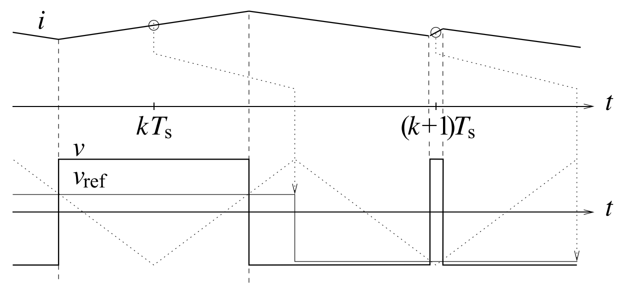

Fig. 3. Single-update PWM, giving $T_d = T_s$.

2) DVC: The purpose of the DVC is to make υ_d track its reference υ_d^{ref}. With $W_d = C_d \upsilon_d^2/2$, the energy balance of the dc link can be expressed as

$$\frac{dW_d}{dt} = \frac{C_d}{2}\frac{d\upsilon_d^2}{dt} = P - P_l \tag{20}$$

where $P = \text{Re}\{\mathbf{S}\}$ and P_l is the load power, including the converter losses ($P_l < 0$ for inverter operation). Since i_d is the active-power-producing current component, the following control law can be used:

$$i_d^{\text{ref}} = F_d(s)\big(W_d^{\text{ref}} - W_d\big), \quad W_d^{\text{ref}} = \frac{C_d\big(\upsilon_d^{\text{ref}}\big)^2}{2}. \tag{21}$$

This allows the DVC to be structurally similar to the PLL controller (17)

$$F_d(s) = \frac{\alpha_d}{E_0}\left(1 + \frac{\alpha_{\text{id}}}{s}\right) \tag{22}$$

and a similar parameter selection recommendation applies, i.e., $\alpha_{\text{id}} < \alpha_d \ll \alpha_c$ (a deviation of the value of C_d used in the control system from the actual value does not give a static control error, but effectively alters α_d).

III. Passivity Properties of the Inner Input Admittance

In this section, the impact of the outer control loops is disregarded, reducing the control system to the CC and the PWM. Yet, the important findings can be made by analyzing this reduced system. Because this system is linear and balanced, such an analysis is relatively straightforward [3]. The total time delay plays an important role at harmonic frequencies. Therefore, the elaborate discussions concerning this parameter are first made.

A. Total Time Delay

In digital VSC control systems, particularly for two-level VSCs, it is useful to sample the converter current synchronously in between switchings, i.e., coinciding with the peaks of the triangular carrier signal for suboscillation PWM, as shown in Fig. 2. Thereby, switching harmonics are suppressed from the samples, often allowing antialiasing filtering to be avoided [35]. There are two variants of this principle.

1) Double-Update PWM: In this variant, samples are taken both at the positive and negative peaks, as shown in Fig. 2. The sampling frequency is twice the switching frequency. The computation time of the CC is generally a fraction of T_s, but it is not negligible. For this reason, it is common practice to delay the update of the phase-voltage reference υ_{ref} (given here without a specific phase notation) by one sampling interval, as shown in Fig. 2 (dotted arrows). The current sample taken at time $t = kT_s$ updates υ_{ref} at $t = (k+1)T_s$, and so on. Thereby, even short pulses, such as that about $t = (k+3)T_s$, can be generated without any error due to computation. Each update of υ_{ref} affects just one switching event, which can occur minimum immediately and maximum T_s after the update. The average (and unavoidable) PWM time delay is $0.5T_s$, which results in the total time delay (on average) $T_d = 1.5T_s$.

2) Single-Update PWM: In this variant, the sampling frequency is set equal to the switching frequency. Consequently, the value of T_s is in this case twice that in double-update PWM (given that the same switching frequency is used in both cases). Current sampling is made either at the positive or negative peaks of the carrier signal, as shown in Fig. 3. Provided that the CC computation time is shorter than $0.5T_s$, reference update can be delayed just until the next peak of the opposite sign (rather than the entire period T_s) [44]. Each update of υ_{ref} affects two switching events, which occur symmetrically about the (in this example, negative) peak. The average PWM time delay taken over two such consecutive switching events is obviously $0.5T_s$, giving $T_d = T_s$.

B. Passivity Properties for Different Total Time Delays

In [2] and [5], it is shown that the negative-real-part region caused by the total time delay begins at the critical frequency f_{crit} at which $\cos\omega T_d$ (for $\omega = 2\pi f_{\text{crit}}$) changes sign from positive to negative, i.e., for $2\pi f_{\text{crit}} T_d = \pi/2$, giving

$$f_{\text{crit}} = \frac{1}{4T_d} = \frac{f_s}{4}\frac{T_s}{T_d}. \tag{23}$$

For double-update PWM and single-update PWM, i.e., respectively, with $T_d = 1.5T_s$ and $T_d = T_s$, we obtain $f_{\text{crit}} = f_s/6$ and $f_{\text{crit}} = f_s/4$, respectively. Let us verify this numerically. A normalized switching frequency of 100 p.u. is considered (with the synchronous frequency as base frequency). This is a reasonable value, accounting for, e.g., a 5-kHz switching frequency at $f_1 = 50$ Hz. Consequently, $\omega_s = 200$ p.u. for double-update PWM and $\omega_s = 100$ p.u.

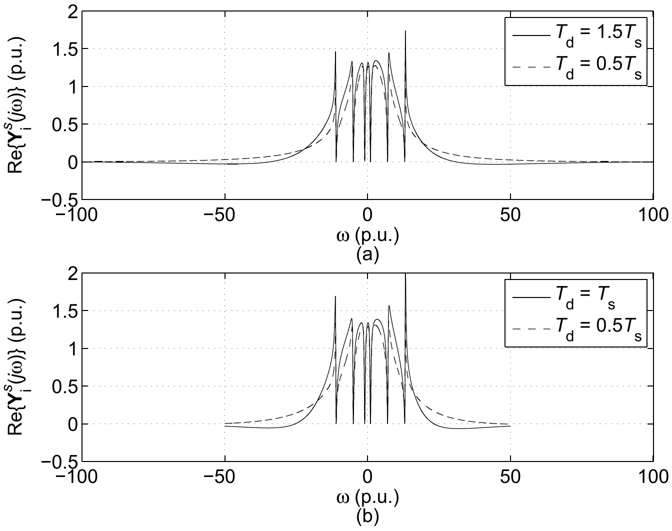

Fig. 4. Real parts of the inner input admittance for (a) double-update PWM and (b) single-update PWM.

for single-update PWM. CC (11) is used, with $\alpha_c = 8$ p.u. Equation (15) shows that this selection yields $\phi_m = 61°$ for single-update PWM with $T_d = T_s$ and $\phi_m = 68°$ for double-update PWM with $T_d = 1.5T_s$, which both are generous values. R parts (ROGIs), with $\alpha_h = 0.2$ p.u. for all h, are included for $+1, -1, -5, +7, -11, +13$ in the $\alpha\beta$ frame, i.e., for $h = 0, -2, \pm 6, \pm 12$ in (5). The R-part compensation angles are selected as a compensation of the time delay at the R-part frequency [4]

$$\phi_h = h\omega_1 T_d. \tag{24}$$

In Fig. 4, the real parts of the inner input admittance are shown in the frequency region up to the Nyquist frequency, i.e., $-\omega_s/2 \leq \omega \leq \omega_s/2$ (since the continuous-time models used here do not account for the effects of aliasing and PWM, evaluation for frequencies above the Nyquist frequency is meaningless). As the solid curves show, for neither one of the PWM variants is a passive system obtained; negative-real-part regions appear above the respective critical frequencies predicted by (23). A proposal for eliminating the negative-real-part region up to the Nyquist frequency for $T_d = 1.5T_s$ by a scheme based on PCC-voltage feedforward can be found in [5]. The scheme can easily be adapted to the case $T_d = T_s$.

If the total time delay can be brought down to $T_d = 0.5T_s$, i.e., just the PWM time delay, then (23) gives $f_{\text{crit}} = f_s/2$, i.e., the negative-real-part region is eliminated and a passive inner input admittance up to the Nyquist frequency is obtained, as verified in Fig. 4 (dashed curves). (This fact is hinted in [40, eq. (6)], but it is not shown explicitly. It is implicitly shown via the Nyquist criterion in [41] and [42].) In addition, α_c can be increased, for a certain ϕ_m, by $1.5/0.5 = 3$ for double-update PWM and by $1/0.5 = 2$ for single-update PWM, as shown by (16).

It is generally easier to reduce T_d to (or close to) $0.5T_s$ for single-update PWM than for double-update PWM [43]–[45]. This is because for single-update PWM, the sampling instant can be shifted between the positive and negative peaks,

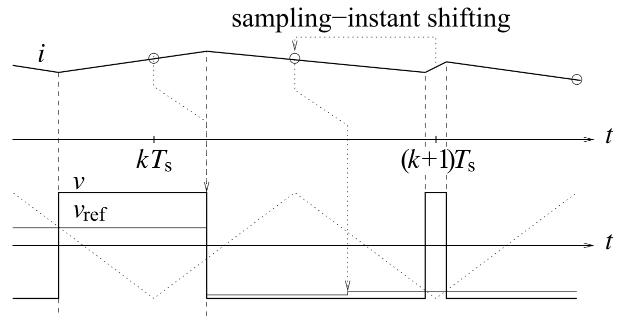

Fig. 5. Single-update PWM with shifting of the sampling instant, giving $T_d = 0.5T_s$.

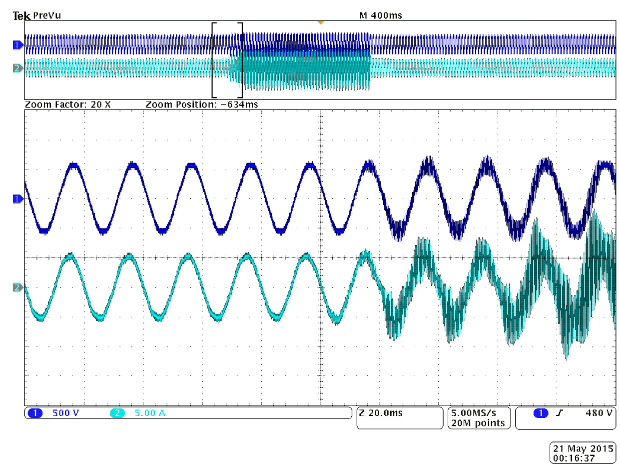

Fig. 6. Experimental results showing (channel 1) the line-to-line (phases a to b) PCC voltage and (channel 2) the phase-a grid current during transition from stable to unstable operation.

as shown in Fig. 5 (where the computational time delay is $\sim 0.2T_s$). When v_{ref} suddenly decreases, the current-sampling instant is shifted from the negative to the positive carrier peak. This allows the short positive pulse about $t = (k+1)T_s$ to be generated without timing error.

For double-update PWM, the sampling instants can be shifted away from the peaks, but at the expense of a greatly increased harmonic content of the current samples [40].

1) Example: Single-update PWM with $f_s = 10$ kHz and $T_d = T_s$ is implemented in the control system for an *LCL*-filter-equipped VSC operating with $f_1 = 50$ Hz. The resonant frequency is 2.1 kHz, i.e., below $f_{\text{crit}} = f_s/4 = 2.5$ kHz. As can be observed in Fig. 6, the system is initially stable. At the center of the displayed time interval, the interrupt for current sampling is shifted, so that $T_d = 1.5T_s$ is obtained, giving $f_{\text{crit}} = f_s/6 = 1.7$ kHz. The resonance now falls within the negative-real-part region, and as a result, growing oscillations commence.

C. Passivity Properties About the R-Part Frequencies

Fig. 7 shows the detail about -11. For the compensation-angle selection (24), $\text{Re}\{\mathbf{Y}_i^s(-j11\omega_1)\}$ is a local minimum, so a local negative-real-part region is avoided, as the solid curve shows. This holds for all R-part frequencies for which $\cos(h\omega_1 T_d) > 0$ and $|h\omega_1| < \omega_s/2$ [4].

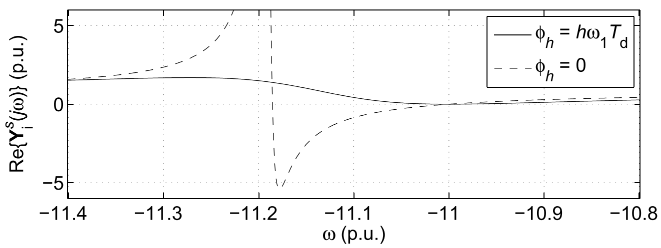

Fig. 7. Real part of the inner input admittance about $h = -11$ for single-update PWM with $T_d = T_s$.

In many publications on proportional-resonant (PR) controllers (including [34]), the feature of a compensation angle is not even included, implying $\phi_h = 0$. In that case, negative-real-part regions appear about the R-part frequencies, as shown in Fig. 7 (dashed curve). Although the regions are narrow, the large negative values obtained for larger $|h|$ may yet be enough to destabilize ill-located grid resonances [4]. Thus, the usage of a properly selected compensation angle is highly recommended.

D. Passivity Properties With PCC-Voltage Feedforward

In [3], it is shown that, if feedforward of the $+1$ component of $\mathbf{E}^s$ is combined with an R part for $+1$ [$h = 0$ in (5)], then a negative-real-part region about $+\omega_1$ results. Caution is thus advised. In addition, (24) needs to be modified, as shown in [4], to prevent negative-real-part regions about the R-part frequencies.

IV. Passivity Properties of the Total Input Admittance

The impact of the PLL and the DVC is now included. The complexity of analysis increases markedly, since the dynamics are nonlinear and imbalanced. Rather than resorting to the usage of a multivariable model, involving real space vectors and transfer matrices [2], [27], modeling is still made using complex space vectors and transfer functions. This method is akin to that in [10], [15], and [17]. The differences are that we elect to use the dq frame rather than a per-phase analysis (thus, obviating the need for deriving separate positive- and negative-sequence expressions), and that the impact of the DVC is considered in addition to the PLL.

A. Impact of the PLL for an $\alpha\beta$-Frame CC

Since a nonlinear system is obtained, linearization must be made to allow transfer functions to be derived. For this sake, a perturbation $\Delta\mathbf{E}$ about the operating point E_0 of the PCC voltage is considered. For a constant ω_1, this yields the $\alpha\beta$-frame vector

$$\mathbf{E}^s = e^{j\omega_1 t}(E_0 + \Delta\mathbf{E}). \tag{25}$$

Introducing a perturbation also in the dq-frame angle, as $\theta = \omega_1 t + \Delta\theta$, gives $\mathbf{E} = e^{-j\theta}\mathbf{E}^s = e^{-j\Delta\theta}(E_0 + \Delta\mathbf{E})$. This relation can be linearized by approximating $e^{-j\Delta\theta} \approx 1 - j\Delta\theta$ and by neglecting cross terms between the perturbation quantities, yielding

$$\mathbf{E} = E_0 + \Delta\mathbf{E} - jE_0\Delta\theta. \tag{26}$$

Substitution of (26) in (18) results in

$$\Delta\theta = \frac{F_p(s)}{s}\mathrm{Im}\{\Delta\mathbf{E}\} - E_0\frac{F_p(s)}{s}\Delta\theta$$
$$\Rightarrow \Delta\theta = \underbrace{\frac{F_p(s)}{s + E_0 F_p(s)}}_{G_p(s)}\mathrm{Im}\{\Delta\mathbf{E}\}. \tag{27}$$

If the integral term of (17) is neglected, then $G_p(s) = [\alpha_p/(s + \alpha_p)]/E_0$, i.e., α_p is the closed-loop PLL bandwidth.

The dq- and $\alpha\beta$-frame CCs (4) and (11) are equivalent under the design premises stated, concerning the current control loop only. However, they differ concerning their PLL impact [15]. For an $\alpha\beta$-frame CC, the dq-frame reference $\mathbf{i}_{\mathrm{ref}}$ is transformed into the $\alpha\beta$ frame as

$$\mathbf{i}^s_{\mathrm{ref}} = e^{j\theta}\mathbf{i}_{\mathrm{ref}} = e^{j(\omega_1 t + \Delta\theta)}(\mathbf{i}_0 + \Delta\mathbf{i}_{\mathrm{ref}}) \tag{28}$$

where $\Delta\mathbf{i}_{\mathrm{ref}}$ is the perturbation about the mean value $\mathbf{i}_0 = i_{d0} + j i_{q0}$. Since a constant $i_q^{\mathrm{ref}} = i_{q0}$ is assumed, $\Delta\mathbf{i}_{\mathrm{ref}} = \Delta i_d^{\mathrm{ref}}$, where $\Delta i_d^{\mathrm{ref}}$ is the perturbation impact from the DVC. Equation (28) can be linearized as

$$\mathbf{i}^s_{\mathrm{ref}} \approx e^{j\omega_1 t}[(1 + j\Delta\theta)\mathbf{i}_0 + \Delta\mathbf{i}_{\mathrm{ref}}] = e^{j\omega_1 t}\left(\mathbf{i}_0 + \Delta\mathbf{i}'_{\mathrm{ref}}\right) \tag{29}$$

where

$$\Delta\mathbf{i}'_{\mathrm{ref}} = \Delta i_d^{\mathrm{ref}} + jG_p(s)\mathbf{i}_0\mathrm{Im}\{\Delta\mathbf{E}\}. \tag{30}$$

The PLL thus acts as an added reference perturbation (in the q-direction only in case $\mathbf{i}_0$ is real). The closed-loop impact of (30) can be determined by considering (6) for the perturbation quantities, i.e.

$$\Delta\mathbf{i} = \mathbf{G}_{\mathrm{ci}}(s)\Delta\mathbf{i}'_{\mathrm{ref}} + \mathbf{Y}_i(s)\Delta\mathbf{E}. \tag{31}$$

Before proceeding to include the DVC, let us discuss the impact just of the PLL by assuming $\Delta i_d^{\mathrm{ref}} = 0$. Since (30) includes $\mathrm{Im}\{\Delta\mathbf{E}\}$, it is obvious that the model no longer is balanced [27]. Yet, a complex space-vector model can be employed using the identity $\mathrm{Im}\{\Delta\mathbf{E}\} = (\Delta\mathbf{E} - \Delta\mathbf{E}^*)/(2j)$ in (30), which gives

$$\Delta\mathbf{i} = \mathbf{Y}_+(s)\Delta\mathbf{E} + \mathbf{Y}_-(s)\Delta\mathbf{E}^* \tag{32}$$

where

$$\mathbf{Y}_+(s) = \mathbf{Y}_i(s) - \mathbf{Y}_-(s), \quad \mathbf{Y}_-(s) = -\frac{\mathbf{G}_{\mathrm{ci}}(s)G_p(s)\mathbf{i}_0}{2}. \tag{33}$$

Equation (32) shows that, if $\Delta\mathbf{E}$ contains just one frequency component, e.g., $\Delta\mathbf{E} = \Delta\mathbf{E}_+ e^{j\omega t}$, then—because of the imbalance—two components appear in $\Delta\mathbf{i}$, as

$$\Delta\mathbf{i} = \underbrace{\mathbf{Y}_+(j\omega)\Delta\mathbf{E}_+ e^{j\omega t}}_{\Delta\mathbf{i}_+} + \underbrace{\mathbf{Y}_-(-j\omega)\Delta\mathbf{E}_+^* e^{-j\omega t}}_{\Delta\mathbf{i}_-}. \tag{34}$$

Component $\Delta\mathbf{i}_-$, which may be called an image [27], is negative sequence in the dq frame, but as long as $\omega < \omega_1$, it is positive sequence in the $\alpha\beta$ frame; the components there appear as sideband components of $+1$, at $\omega_1 \pm \omega$.

Both components, in turn, affect $\Delta\mathbf{E}$ via the negative feedback described by (3). If $\mathbf{Z}(s)$ has a resonance at, or close to, $+\omega$, then $\Delta\mathbf{i}_+$ will be amplified, giving a large amplitude $|\Delta\mathbf{E}_+|$ (initially exponentially growing if the resonance gets destabilized). Because the grid is assumed to be balanced, $|\mathbf{Z}^s(-j\omega)| = |\mathbf{Z}^s(j\omega)|$, whereas $|\mathbf{Z}(-j\omega)| \neq |\mathbf{Z}(j\omega)|$ for $\omega \neq 0$. Consequently, $\Delta\mathbf{i}_-$ is amplified much less by the resonance than $\Delta\mathbf{i}_+$. The dominant component of $\Delta\mathbf{E}$ is still $\Delta\mathbf{E}_+ e^{j\omega t}$. This component may produce active power of nonzero mean with $\Delta\mathbf{i}_+$, according to $\text{Re}\{\Delta\mathbf{E}_+ e^{j\omega t}\Delta\mathbf{i}_+^*\} = \text{Re}\{\mathbf{Y}_+(j\omega)\}|\Delta\mathbf{E}_+|^2$, whereas its interaction with $\Delta\mathbf{i}_-$ just produces active-power pulsations of the angular frequency 2ω. This motivates neglecting the impact of $\mathbf{Y}_-(s)$ for a stability analysis of the converter-grid interconnection for a balanced grid. Caution is advised, though, since in certain degenerated cases the assumptions may not hold. Moreover, for interaction with an imbalanced grid, which is the case, e.g., for subsynchronous torsional interaction [33] and analysis of multiple-converter systems, a multivariable model, as in [2], must be used.

Similar conclusions are drawn in [10], [15], and [17], though using somewhat different motivations and a different linearization method. In addition, the per-phase analysis is used, which does not allow the existence of an image component to be revealed.

B. Impact of the DVC

We now proceed to determine the impact of the DVC. Combining (20) with (21) and the relation $P = \text{Re}\{\mathbf{E}\mathbf{i}^*\} = \text{Re}\{\mathbf{E}^*\mathbf{i}\}$ yields

$$i_d^{\text{ref}} = F_d(s)\left[W_d^{\text{ref}} - \frac{\text{Re}\{(E_0 + \Delta\mathbf{E})^*(\mathbf{i}_0 + \Delta\mathbf{i})\} - P_l}{s}\right] \quad (35)$$

which can be linearized as

$$\Delta i_d^{\text{ref}} = -\frac{F_d(s)}{s}\text{Re}\{E_0\Delta\mathbf{i} + \mathbf{i}_0\Delta\mathbf{E}^*\}. \quad (36)$$

Substitution of (31) in (36), noting that $\text{Re}\{\mathbf{i}_0\Delta\mathbf{E}^*\} = \text{Re}\{\mathbf{i}_0^*\Delta\mathbf{E}\}$, yields

$$\Delta i_d^{\text{ref}} = -\frac{F_d(s)}{s}\text{Re}\big\{E_0\big[\mathbf{G}_{\text{ci}}(s)\Delta\mathbf{i}'_{\text{ref}} + \mathbf{Y}_i(s)\Delta\mathbf{E}\big] + \mathbf{i}_0^*\Delta\mathbf{E}\big\}. \quad (37)$$

This relation has, due to the real part of $\Delta\mathbf{i}'_{\text{ref}}$, Δi_d^{ref} on both sides. To allow solving for Δi_d^{ref}, the approximation $\mathbf{G}_{\text{ci}}(s) \approx 1$ is made. Since $\alpha_c \gg \alpha_d$, frequency components outside the passband of $\mathbf{G}_{\text{ci}}(s)$ are well attenuated by $F_d(s)/s$, so neglecting the filtering effect of $\mathbf{G}_{\text{ci}}(s)$ is reasonable. We thus obtain

$$\Delta i_d^{\text{ref}} \approx -\frac{F_d(s)}{s}\text{Re}\left\{E_0\Delta\mathbf{i}'_{\text{ref}} + [E_0\mathbf{Y}_i(s) + \mathbf{i}_0^*]\Delta\mathbf{E}\right\} \quad (38)$$

where, from (30), $\text{Re}\{\Delta\mathbf{i}'_{\text{ref}}\} = \Delta i_d^{\text{ref}} - i_{q0}G_p(s)\text{Im}\{\Delta\mathbf{E}\}$. For brevity, we shall neglect the term $-i_{q0}G_p(s)\text{Im}\{\Delta\mathbf{E}\}$, which tends to have a small impact, particularly at high power factors. This allows (38) to be simplified to

$$\Delta i_d^{\text{ref}} = -\underbrace{\frac{F_d(s)}{s + E_0F_d(s)}}_{G_d(s)}\text{Re}\{[E_0\mathbf{Y}_i(s) + \mathbf{i}_0^*]\Delta\mathbf{E}\}. \quad (39)$$

If the integral term of (22) is neglected, then $G_d(s) = [\alpha_d/(s+\alpha_d)]/E_0$, i.e., α_d is the bandwidth of the direct-voltage control loop. The complete relation between $\Delta\mathbf{E}$ and $\Delta\mathbf{i}$, including PLL and DVC impact, can now be obtained by substituting (39) in (30) and using the identities $\text{Re}\{\Delta\mathbf{E}\} = (\Delta\mathbf{E}+\Delta\mathbf{E}^*)/2$ and $\text{Im}\{\Delta\mathbf{E}\} = (\Delta\mathbf{E} - \Delta\mathbf{E}^*)/(2j)$. The result is identical to (32), but with

$$\mathbf{Y}_+(s) = \mathbf{Y}_i(s) + \frac{\mathbf{G}_{\text{ci}}(s)}{2}\{G_p(s)\mathbf{i}_0 - G_d(s)[\mathbf{i}_0^* + E_0\mathbf{Y}_i(s)]\} \quad (40)$$

[as $\mathbf{Y}_-(s)$ is not used in the following, its expression is omitted].

Remark 5: As previously mentioned, the control loop for the PCC-voltage magnitude or the reactive power is disregarded in order to save space. However, inclusion in the analysis of its impact is straightforward. For example, a PCC-voltage-magnitude control law $i_q^{\text{ref}} = F_a(s)(E_0 - |\mathbf{E}|)$ can be shown to add a term $-j\mathbf{G}_{\text{ci}}(s)F_a(s)/2$ to (40).

C. Impact of the PLL for a dq-Frame CC

A different impact of the PLL on the total input admittance is obtained for a dq-frame CC than for an $\alpha\beta$-frame CC [46]. This is because two coordinate transformations, of $\mathbf{i}^s$ into the dq frame and of $\mathbf{v}_{\text{ref}}$ into the $\alpha\beta$ frame, are used, thus adding two sources of PLL impact. Straightforward calculations show that this adds a term $-\mathbf{Y}_i(s)G_p(s)/2$ to (40).

D. Examples of Passivity Properties Versus Resonance Destabilization

We shall now, by two examples, correlate numerically the passivity properties of $\mathbf{Y}_+(s)$ given by (40) with the occurrences of resonance destabilization found by simulation in MATLAB. The grid impedance is selected as a parallel–series inductive–capacitive impedance

$$\mathbf{Z}^s(s) = sL_g||\left(sL_s + \frac{1}{sC_s}\right) = \frac{sL_g(s^2L_sC_s + 1)}{s^2(L_g + L_s)C_s + 1} \quad (41)$$

i.e., the angular resonant frequency in the $\alpha\beta$ frame is $\omega_{\text{res}} = 1/((L_g + L_s)C_s)^{1/2}$. $L_g = L = 0.1$ p.u. and $L_s = 1$ p.u. are selected, whereas C_s is varied in order to obtain the desired ω_{res}, as explained in the following. In the control system—which uses an $\alpha\beta$-frame CC—an R part is included only for $+1$, i.e., for $h = 0$ in (5), with $\alpha_h = 0.5$ p.u. The PLL and the DVC have the parameters $\alpha_p = \alpha_d = 0.2$ p.u. and $\alpha_{\text{ip}} = \alpha_{\text{id}} = 0.05$ p.u., except where noted otherwise. The grid voltage is adjusted so as to give $E_0 = 1$ p.u., the reactive-power exchange is zero, i.e., $i_{q0} = 0$, and the system is considered lossless. The last two assumptions yield $\mathbf{i}_0 = P_l/E_0$.

1) Example 1: Inverter Operation: A power injection $P_l = -0.9$ p.u. into the dc link is considered. This scenario could account for, e.g., a photovoltaic inverter. To allow the PLL to quickly track variations in the PCC-voltage angle, $\alpha_p = 2$ p.u. is used in this example (see [10] for a similar selection). The angular resonant frequency ω_{res} is adjusted

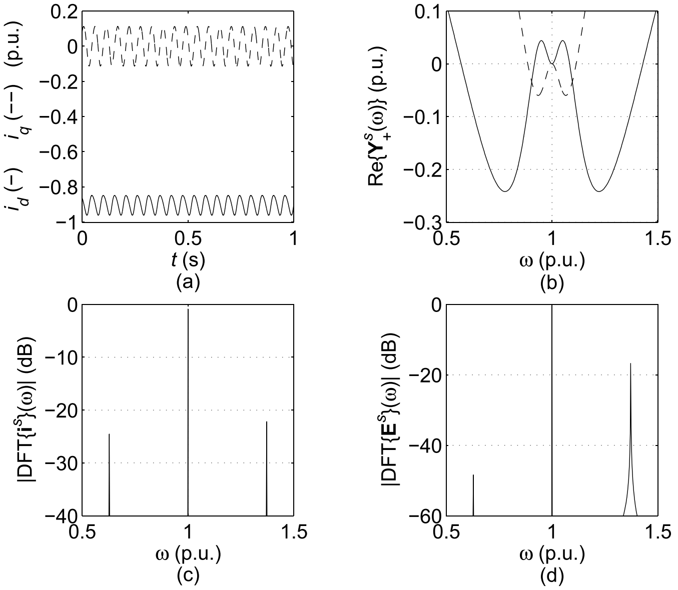

Fig. 8. Inverter operation with $\omega_{\mathrm{res}} = 1.38$ p.u. (a) Converter-current components. (b) Input-admittance real parts, where the dashed curve accounts for rectifier operation with $P_l = 0.9$ p.u. (c) DFT of the converter current. (d) DFT of the PCC voltage.

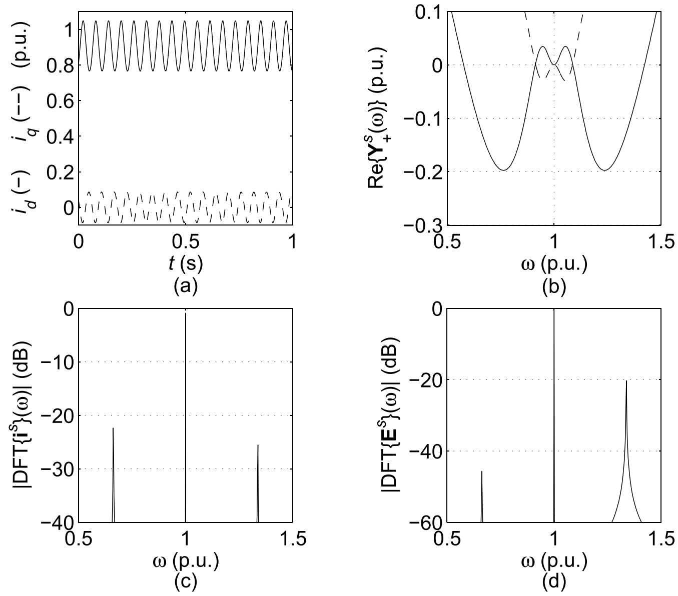

Fig. 9. Rectifier operation with $\omega_{\mathrm{res}} = 1.34$ p.u. (a) Converter-current components. (b) Input-admittance real parts, where the dashed curve accounts for inverter operation with $P_l = -0.9$ p.u. (c) DFT of the converter current. (d) DFT of the PCC voltage.

until marginally stable operation is reached, i.e., a constant-amplitude oscillation occurs, as shown in Fig. 8(a). This correlates well with Fig. 8(b), where the real part of $\mathbf{Y}^s_+(s) = \mathbf{Y}_+(s - j\omega_1)$ is shown: $\omega_{\mathrm{res}} = 1.38$ p.u. is located near the upper boundary of the negative-real-part region. Fig. 8(c) shows the discrete Fourier transform (DFT) modulus of $\mathbf{i}^s$ in a logarithmic scale. The components $|\mathbf{i}^s_+|$ and $|\mathbf{i}^s_-|$, located symmetrically about $\omega_1 = 1$ p.u., at ω_{res} and $2\omega_1 - \omega_{\mathrm{res}}$, respectively, can be observed. The corresponding components in $\mathbf{E}^s$ are shown in Fig. 8(d). It can be noted that the lower sideband component has roughly 30 dB smaller amplitude than the upper sideband component, and therefore can be neglected, as discussed in Section IV-A.

The PLL gives a negative impact for inverter operation [2], which can be deduced by the multiplication by $\mathbf{i}_0$ of $G_p(s)$ in (40). The dashed curve in Fig. 8(b) shows that a much smaller negative-real-part region is obtained for rectifier operation with the same parameter values. For inverter operation, α_p should not be made larger than necessary to obtain acceptable dynamic performance, in order to minimize the negative-real-part region.

2) Example 2 *(Rectifier Operation):* A power draw of $P_l = 0.9$ p.u. from the dc link is now considered. This scenario could account for, e.g., a back-to-back ac motor drive. To give sufficiently small variations in v_d for variations that may occur in P_l (though not included in the simulation), a larger $\alpha_d = 0.5$ p.u. is this time used. The results shown in Fig. 9 are very similar to those in Fig. 8, although the negative-real-part region this time is slightly smaller. Consequently, a slightly lower ω_{res} is needed to give marginally stable operation.

The DVC gives negative impact mainly for rectifier operation [2], which can be deduced by the multiplication by $-\mathbf{i}^*_0$ of $G_d(s)$ in (40). The dashed curve in Fig. 9(b) shows that a much smaller negative-real-part region is obtained for inverter operation with the same parameter values. For rectifier operation, α_d should not be made larger than necessary to obtain acceptable dynamic performance, in order to minimize the negative-real-part region.

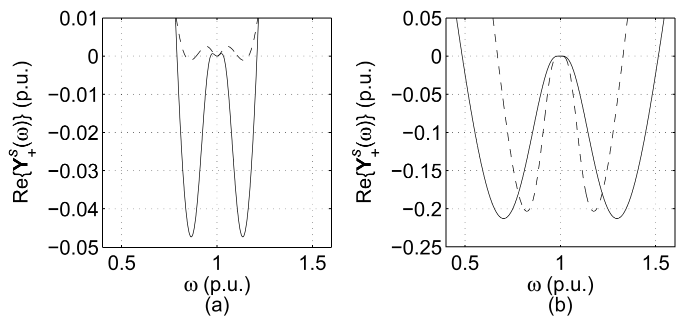

Fig. 10. Input-admittance real parts for (a) $\alpha\beta$-frame CC and (b) dq-frame CC for (solid lines) $\alpha_p = \alpha_d = 0.5$ p.u. and (dashed lines) $\alpha_p = \alpha_d = 0.2$ p.u.

Remark 6: It is interesting to note in (40) that, for $G_p(s) = G_d(s)$ and a real $\mathbf{i}_0$, terms $G_p(s)\mathbf{i}_0$ and $-G_d(s)\mathbf{i}^*_0$ cancel in (40). Thus, the identical selections of the PLL controller (17) and the DVC (22) remove the dependence of i_{d0} from the input-admittance characteristics, giving the same passivity properties for both inverter and rectifier operations. For moderate gain selections, then very small negative-real-part regions are obtained, as shown in Fig. 10(a).

Remark 7: If a dq-frame CC is used, a widening of the negative-real-part region tends to result, as shown in Fig. 10(b). It is, therefore, generally preferable to use an $\alpha\beta$-frame CC.

V. Conclusion

An overview of methods for stability assessment based on the passivity properties of the VSC input admittance was presented. The modeling and analysis method in [10], [15], and [17] was generalized. Design recommendations for minimizing the negative-real-part regions were derived. These recommendations, which, in terms of passivity properties, clarify the key results of papers cited in the text, can be summarized as follows:

1) make the total time delay T_d as small as possible. If it can be made equal just to the PWM time delay $0.5T_s$ [40]–[42], then a positive real part of the inner input admittance is obtained up to the Nyquist frequency;
2) use proper selection of the R-part compensation angles ϕ_h according to (24), particularly if R parts are included for higher harmonic orders [4];
3) do not select the bandwidths of the outer loops, i.e., the PLL and the DVC, unnecessarily large, this particularly applies for the PLL in inverter operation and the DVC in rectifier operation [2], [11], [23];
4) use an $\alpha\beta$-frame CC to reduce the PLL impact [46].

References

[1] B. K. Bose, "Global energy scenario and impact of power electronics in 21st century," *IEEE Trans. Ind. Electron.*, vol. 60, no. 7, pp. 2638–2651, Jul. 2013.

[2] L. Harnefors, M. Bongiorno, and S. Lundberg, "Input-admittance calculation and shaping for controlled voltage-source converters," *IEEE Trans. Ind. Electron.*, vol. 54, no. 6, pp. 3323–3334, Dec. 2007.

[3] L. Harnefors, L. Zhang, and M. Bongiorno, "Frequency-domain passivity-based current controller design," *IET Power Electron.*, vol. 1, no. 4, pp. 455–465, Dec. 2008.

[4] L. Harnefors, A. G. Yepes, A. Vidal, and J. Doval-Gandoy, "Passivity-based stabilization of resonant current controllers with consideration of time delay," *IEEE Trans. Power Electron.*, vol. 29, no. 12, pp. 6260–6263, Dec. 2014.

[5] L. Harnefors, A. G. Yepes, A. Vidal, and J. Doval-Gandoy, "Passivity-based controller design of grid-connected VSCs for prevention of electrical resonance instability," *IEEE Trans. Ind. Electron.*, vol. 62, no. 2, pp. 702–710, Feb. 2015.

[6] A. A. A. Radwan and Y. A.-R. I. Mohamed, "Assessment and mitigation of interaction dynamics in hybrid AC/DC distribution generation systems," *IEEE Trans. Smart Grid*, vol. 3, no. 3, pp. 1382–1393, Sep. 2012.

[7] X. Wang, F. Blaabjerg, and P. C. Loh, "Proportional derivative based stabilizing control of paralleled grid converters with cables in renwable power plants," in *Proc. IEEE Energy Convers. Congr. Expo. (ECCE)*, Sep. 2014, pp. 4917–4924.

[8] F. Wang, J. L. Duarte, M. A. M. Hendrix, and P. F. Ribeiro, "Modeling and analysis of grid harmonic distortion impact of aggregated DG inverters," *IEEE Trans. Power Electron.*, vol. 26, no. 3, pp. 786–797, Mar. 2011.

[9] J. Sun, "Impedance-based stability criterion for grid-connected inverters," *IEEE Trans. Power Electron.*, vol. 26, no. 11, pp. 3075–3078, Nov. 2011.

[10] M. Céspedes and J. Sun, "Modeling and mitigation of harmonic resonance between wind turbines and the grid," in *Proc. IEEE Energy Convers. Congr. Expo. (ECCE)*, Sep. 2011, pp. 2109–2116.

[11] M. Céspedes and J. Sun, "Impedance shaping of three-phase grid-parallel voltage-source converters," in *Proc. 27th Annu. IEEE Appl. Power Electron. Conf. Expo. (APEC)*, Feb. 2012, pp. 754–760.

[12] S. Vesti, T. Suntio, J. A. Oliver, R. Prieto, and J. A. Cobos, "Impedance-based stability and transient-performance assessment applying maximum peak criteria," *IEEE Trans. Power Electron.*, vol. 28, no. 5, pp. 2099–2104, May 2013.

[13] N. Bottrell, M. Prodanovic, and T. C. Green, "Dynamic stability of a microgrid with an active load," *IEEE Trans. Power Electron.*, vol. 28, no. 11, pp. 5107–5119, Nov. 2013.

[14] R. Turner, S. Walton, and R. Duke, "A case study on the application of the Nyquist stability criterion as applied to interconnected loads and sources on grids," *IEEE Trans. Ind. Electron.*, vol. 60, no. 7, pp. 2740–2749, Jul. 2013.

[15] M. Céspedes and J. Sun, "Impedance modeling and analysis of grid-connected voltage-source converters," *IEEE Trans. Power Electron.*, vol. 29, no. 3, pp. 1254–1261, Mar. 2014.

[16] X. Wang, F. Blaabjerg, M. Liserre, Z. Chen, J. He, and Y. Li, "An active damper for stabilizing power-electronics-based AC systems," *IEEE Trans. Power Electron.*, vol. 29, no. 7, pp. 3318–3329, Jul. 2014.

[17] M. Céspedes and J. Sun, "Mitigation of inverter-grid harmonic resonance by narrow-band damping," *IEEE J. Emerg. Sel. Topics Power Electron.*, vol. 2, no. 4, pp. 1024–1031, Dec. 2014.

[18] X. Wang, F. Blaabjerg, and W. Wu, "Modeling and analysis of harmonic stability in an AC power-electronics-based power system," *IEEE Trans. Power Electron.*, vol. 29, no. 12, pp. 6421–6432, Dec. 2014.

[19] C. Wan, M. Huang, C. K. Tse, and X. Ruan, "Effects of interaction of power converters coupled via power grid: A design-oriented study," *IEEE Trans. Power Electron.*, vol. 30, no. 7, pp. 3589–3600, Jul. 2015.

[20] Y. Tao, Q. Liu, Y. Deng, X. Liu, and X. He, "Analysis and mitigation of inverter output impedance impacts for distributed energy resource interface," *IEEE Trans. Power Electron.*, vol. 30, no. 7, pp. 3563–3576, Jul. 2015.

[21] X. Wang, Y. Pang, P. C. Loh, and F. Blaabjerg, "A series-LC-filtered active damper with grid disturbance rejection for AC power-electronics-based power systems," *IEEE Trans. Power Electron.*, vol. 30, no. 8, pp. 4037–4041, Aug. 2015.

[22] X. Wang, Y. W. Li, F. Blaabjerg, and P. C. Loh, "Virtual-impedance-based control for voltage-source and current-source converters," *IEEE Trans. Power Electron.*, vol. 30, no. 12, pp. 7019–7037, Dec. 2015.

[23] B. Wen, D. Boroyevich, R. Burgos, P. Mattavelli, and Z. Shen, "Analysis of D-Q small-signal impedance of grid-tied inverters," *IEEE Trans. Power Electron.*, vol. 31, no. 1, pp. 675–687, Jan. 2016.

[24] P. M. Anderson, B. L. Agrawal, and J. E. Van Ness, *Subsynchronous Resonance in Power Systems*. New York, NY, USA: IEEE Press, 1990.

[25] M. Aeberhard, M. Meyer, and C. Courtois, "The new standard EN 50388-2, Part 2—Stability and harmonics," *Elektrische Bahnen*, vol. 12, no. 1, pp. 28–35, 2014.

[26] D. Dujic *et al.*, "Power electronic traction transformer-low voltage prototype," *IEEE Trans. Power Electron.*, vol. 28, no. 12, pp. 5522–5534, Dec. 2013.

[27] L. Harnefors, "Modeling of three-phase dynamic systems using complex transfer functions and transfer matrices," *IEEE Trans. Ind. Electron.*, vol. 54, no. 4, pp. 2239–2248, Aug. 2007.

[28] M. Meyer and J. Schöning, "Netzstabilität in grossen Bahnnetzen," (in German), *Eisenbahn-Revue Int.*, nos. 7–8, pp. 312–317, 1999.

[29] A. D. B. Paice and M. Meyer, "Rail network modelling and stability: The input admittance criterion," in *Proc. 14th Int. Symp. Math. Theory Netw. Syst.*, Perpignan, France, Jun. 2000, pp. 1–6.

[30] E. Möllerstedt and B. Bernhardsson, "Out of control because of harmonics—An analysis of the harmonic response of an inverter locomotive," *IEEE Control Syst. Mag.*, vol. 20, no. 4, pp. 70–81, Aug. 2000.

[31] M. Jansson, A. Danielsson, J. Galić, K. Pietiäinen, and L. Harnefors, "Stable and passive traction drives," in *Proc. IEEE Nordic Power Ind. Electron. Conf.*, Trondheim, Norway, Jun. 2004, pp. 1–6.

[32] N. P. W. Strachan and D. Jovcic, "Stability of a variable-speed permanent magnet wind generator with weak AC grids," *IEEE Trans. Power Del.*, vol. 25, no. 4, pp. 2779–2788, Oct. 2010.

[33] L. Harnefors, "Analysis of subsynchronous torsional interaction with power electronic converters," *IEEE Trans. Power Syst.*, vol. 22, no. 1, pp. 305–313, Feb. 2007.

[34] C. A. Busada, S. Gómez Jorge, A. E. Leon, and J. A. Solsona, "Current controller based on reduced order generalized integrators for distributed generation systems," *IEEE Trans. Ind. Electron.*, vol. 59, no. 7, pp. 2898–2909, Jul. 2012.

[35] S. Buso and P. Mattavelli, *Digital Control in Power Electronics*. San Rafael, CA, USA: Morgan & Claypool, 2006.

[36] P. Mattavelli, "Synchronous-frame harmonic control for high-performance AC power supplies," *IEEE Trans. Ind. Appl.*, vol. 37, no. 3, pp. 864–872, May/Jun. 2001.

[37] D. G. Holmes, T. A. Lipo, B. P. McGrath, and W. Y. Kong, "Optimized design of stationary frame three phase AC current regulators," *IEEE Trans. Power Electron.*, vol. 24, no. 11, pp. 2417–2426, Nov. 2009.

[38] L. Harnefors and H.-P. Nee, "Model-based current control of AC machines using the internal model control method," *IEEE Trans. Ind. Appl.*, vol. 34, no. 1, pp. 133–141, Jan./Feb. 1998.

[39] H. Akagi, E. H. Watanabe, and M. Aredes, *Instantaneous Power Theory and Applications to Power Conditioning*. New York, NY, USA: Wiley, 2007.

[40] D. Pan, X. Ruan, C. Bao, W. Li, and X. Wang, "Capacitor-current-feedback active damping with reduced computation delay for improving robustness of LCL-type grid-connected inverter," *IEEE Trans. Power Electron.*, vol. 29, no. 7, pp. 3414–3427, Jul. 2014.

[41] C. Zou, B. Liu, S. Duan, and R. Li, "Influence of delay on system stability and delay optimization of grid-connected inverters with LCL filter," *IEEE Trans. Ind. Informat.*, vol. 10, no. 3, pp. 1775–1784, Aug. 2014.

[42] J. Wang, J. Yan, L. Jiang, and J. Zou, "Delay-dependent stability of single-loop controlled grid-connected inverters with LCL filters," *IEEE Trans. Power Electron.*, vol. 31, no. 1, pp. 743–757, Jan. 2016.

[43] H. Deng, R. Oruganti, and D. Srinivasan, "PWM methods to handle time delay in digital control of a UPS inverter," *IEEE Power Electron Lett.*, vol. 3, no. 1, pp. 1–6, Mar. 2005.

[44] P. Mattavelli, F. Polo, F. Dal Lago, and S. Saggini, "Analysis of control-delay reduction for the improvement of UPS voltage-loop bandwidth," *IEEE Trans. Ind. Electron.*, vol. 55, no. 8, pp. 2903–2911, Aug. 2008.

[45] D. Yang, X. Ruan, and H. Wu, "A real-time computation method with dual sampling mode to improve the current control performance of the *LCL*-type grid-connected inverter," *IEEE Trans. Ind. Electron.*, vol. 62, no. 7, pp. 4563–4572, Jul. 2015.

[46] B. Wen, D. Boroyevich, R. Burgos, and P. Mattavelli, "Input impedance of voltage source converter with stationary frame linear current regulators and phase-locked loop," in *Proc. IEEE Energy Convers. Congr. Expo. (ECCE)*, Sep. 2013, pp. 4207–4213.

Lennart Harnefors (S'93–M'97–SM'07) was born in Eskilstuna, Sweden, in 1968. He received the M.Sc., Licentiate, and Ph.D. degrees in electrical engineering from the Royal Institute of Technology (KTH), Stockholm, Sweden, in 1993, 1995, and 1997, respectively, and the Docent degree in industrial automation from Lund University, Lund, Sweden, in 2000.

He was with Mälardalen University, Västerås, Sweden, from 1994 to 2005, where he was appointed as a Professor in 2001. From 2001 to 2005, he was, in addition, a part-time Visiting Professor of Electrical Drives with the Chalmers University of Technology, Gothenburg, Sweden. Since 2005, he has been with ABB, where he is currently a Senior Principal Scientist with Corporate Research, Västerås. He is, in addition, a part-time Adjunct Professor of Power Electronics with KTH. His current research interests include analysis and control of power electronic systems, in particular, grid connected converters and ac drives.

Xiongfei Wang (S'10–M'13) received the B.Sc. degree in electrical engineering from Yanshan University, Qinhuangdao, China, in 2006, the M.Sc. degree from the Harbin Institute of Technology, Harbin, China, in 2008, and the Ph.D. degree from Aalborg University, Aalborg, Denmark, in 2013.

He has been with Aalborg University since 2009, where he is currently an Assistant Professor with the Department of Energy Technology. His current research interests include grid converters for renewable energy systems and microgrids, harmonics analysis and control, passive and active filters, and stability of power electronic-based power systems.

Dr. Wang received the IEEE Power Electronics Transactions Second Prize Paper Award in 2015. He is an Associate Editor of the IEEE TRANSACTIONS ON INDUSTRY APPLICATIONS, and served as a Guest Associate Editor of the IEEE JOURNAL OF EMERGING AND SELECTED TOPICS IN POWER ELECTRONICS of the Special Issue on Harmonic Stability and Mitigation in Power Electronics Based Power Systems.

Alejandro G. Yepes (S'10–M'12) received the M.Sc. and Ph.D. degrees from the University of Vigo, Vigo, Spain, in 2009 and 2011, respectively.

He has been with the Department of Electronics Technology, University of Vigo, since 2008. His current research interests include control of switching power converters.

Frede Blaabjerg (S'86–M'88–SM'97–F'03) was with ABB-Scandia, Randers, Denmark, from 1987 to 1988. From 1988 to 1992, he was a Ph.D. Student with Aalborg University, Aalborg, Denmark. He became an Assistant Professor in 1992, an Associate Professor in 1996, and a Full Professor of Power Electronics and Drives in 1998. His current research interests include power electronics and its applications, such as in wind turbines, PV systems, reliability, harmonics, and adjustable speed drives.

Dr. Blaabjerg has received 15 IEEE Prize Paper Awards. He received the IEEE PELS Distinguished Service Award in 2009, the EPE-PEMC Council Award in 2010, the IEEE William E. Newell Power Electronics Award in 2014, and the Villum Kann Rasmussen Research Award in 2014. He was the Editor-in-Chief of the IEEE TRANSACTIONS ON POWER ELECTRONICS from 2006 to 2012. He was a Distinguished Lecturer of the IEEE Power Electronics Society from 2005 to 2007, and the IEEE Industry Applications Society from 2010 to 2011. He was nominated between the most 250 cited researchers in engineering in the world by Thomson Reuters in 2014.